Available online at www.sciencedirect.com
ScienceDirect
Journal of Sound and Vibration 299 (2007) 314–330
JOURNAL OF SOUND AND VIBRATION
www.elsevier.com/locate/jsvi

Thermally induced transitions to chaos in plate vibrations

P. Ribeiro*

IDMEC/DEMEGI, Faculdade de Engenharia da Universidade do Porto, R. Dr. Roberto Frias, s/n, 4200-465 Porto, Portugal

Received 6 April 2006; received in revised form 11 July 2006; accepted 10 August 2006
Available online 26 September 2006

Abstract

The geometrically nonlinear vibrations of linear elastic and isotropic plates under the combined effect of thermal fields and mechanical excitations are analysed. With this purpose, a model based on a *p*-version, hierarchical, first-order shear deformation finite element is employed. The equations of motion are solved in the time domain by Newmark's implicit time integration method. The temperature and the amplitude of the mechanical excitation are varied, and transitions from periodic to non-periodic motions are found.

1. Introduction

Nonlinear, large amplitude, oscillations of plates subjected to thermal fields and external mechanical excitations are frequent and an important problem in engineering [1]. This problem is also a very interesting one, among other reasons because buckling may occur due to the thermal forces. Thus, different aspects related with this topic have been analysed before, as briefly described in the review that follows.

The finite element method (FEM) was used in Ref. [2] to simulate the geometrically nonlinear oscillations of laminated composite plates and shells under the action of heat loads; non-periodic motions were found, with large growth in the vibration amplitude. In Ref. [3], Murphy et al. analysed the response of a thermally and acoustically loaded plate, following classical, thin plate theory and applying Galerkin's method. Periodic and non-periodic motions were found. Mei and co-workers used the finite element method in several studies devoted to geometrically nonlinear vibrations of panels with thermal fields (Refs. [4–6], for example). The FEM and modal coordinate concept were combined, a procedure that allows one to model complicated geometries with a reduced number of degrees of freedom. A theoretical and experimental study of thermal buckling of clamped, rectangular plates was carried out in Ref. [7]. Although only buckling was analysed, the conclusions achieved are of some importance in dynamics: it was concluded that the plate aspect ratio is not sufficient to describe the problem uniquely, since both the edge length to thickness ratios (a/h and b/h) are independent parameters. Experimental difficulties were met due to the real plate initial curvature. In Ref. [8]

*Tel.: +351 22 508 17 16; fax: +351 22 508 14 45.
E-mail address: pmleal@fe.up.pt.

0022-460X/$ - see front matter © 2006 Elsevier Ltd. All rights reserved.
doi:10.1016/j.jsv.2006.08.003

the dynamic stability of infinitely wide composite plates subjected to suddenly applied thermal or mechanical loads was investigated. It was found that small variations in the temperature can lead to large variations in the oscillations amplitude. Chen and Virgin [9] used finite element and Galerkin approaches to analyse a thermally loaded simply supported plate. Thin plate theory was followed; the static behaviour and natural mode shapes of vibration were investigated.

In this paper, the very efficient *p*-version, hierarchical finite element derived in Ref. [10] is employed to analyse the geometrically nonlinear vibration of plates under thermal fields and mechanical excitations. The approach proposed offers the benefits of lower computational cost, when compared with the *h*-version FEM, but maintains the accuracy and versatility of the FEM. It is intended to find conditions for the occurrence of different types of oscillations, by varying the temperature, damping and excitation amplitude. Plates in linear elastic and isotropic materials are considered and the temperature is uniform in the plate domain. The plate boundaries are fixed; therefore, the temperature variations introduce thermal forces and may cause buckling. The equations of motion are solved by direct numerical integration, using Newmark's method, and different types of oscillations are found.

2. Formulation

The displacement components along the in-plane x and y directions—displacements $u(x, y, z, t)$, $v(x, y, z, t)$—at any point of the plate are assumed to be functions of the middle surface membrane translations $u^0(x, y, t)$, $v^0(x, y, t)$, and of the independent rotations of normals to the middle surface about the x- and y-axis [11], which are respectively denoted by $\theta_x^0(x, y, t)$ and $\theta_y^0(x, y, t)$. Hence, the displacements are given by

$$u(x, y, z, t) = u^0(x, y, t) + z\theta_y^0(x, y, t), \tag{1}$$

$$v(x, y, z, t) = v^0(x, y, t) - z\theta_x^0(x, y, t), \tag{2}$$

$$w(x, y, z, t) = w^0(x, y, t), \tag{3}$$

where $w(x, y, z, t)$ is the displacement in the transverse, z direction.

In each element, the middle plane displacements depend on the local coordinates ξ, η, expressed through the shape functions matrix $\mathbf{N}(\xi, \eta)$, and on the vector of generalized displacements $\mathbf{q}(t) = \{\mathbf{q_u}(\mathbf{t}), \mathbf{q_v}(\mathbf{t}), \mathbf{q_w}(\mathbf{t}), \mathbf{q}_{\theta_x}(\mathbf{t}), \mathbf{q}_{\theta_y}(\mathbf{t})\}$:

$$\begin{Bmatrix} u^0(\xi, \eta, t) \\ v^0(\xi, \eta, t) \\ w^0(\xi, \eta, t) \\ \theta_x^0(\xi, \eta, t) \\ \theta_y^0(\xi, \eta, t) \end{Bmatrix} = \mathbf{N}(\xi, \eta)\mathbf{q}(t). \tag{4}$$

Vectors and matrices are represented by bold upright letters, however; when sub-components of vectors and matrices are distinguished, {} is used for column vector and [ ] for matrix. To improve the accuracy of the approximation, the number and the order of the shape functions are increased. Details on this approach, including the shape functions used, may be found in Refs. [10,12] and references therein. Henceforth, the representation of functions will be simplified: for example $u^0(\xi, \eta, t)$ will be represented simply as u^0.

The temperature field is in fact coupled with the elastic strain field and the theory of thermoelasticity [13] may be used to study this coupling. However, for relatively thin plates and if both plate faces have the same temperature, it is generally accurate to assume that the temperature is uniform in all the plate.

In this case, the constitutive equations for linear elastic isotropic materials, including thermal effects [1], are the following:

$$\begin{Bmatrix} \sigma_x \\ \sigma_y \\ \sigma_{yz} \\ \sigma_{xz} \\ \sigma_{xy} \end{Bmatrix} = \frac{E}{(1+v)} \begin{bmatrix} \frac{1}{1-v} & \frac{v}{1-v} & 0 & 0 & 0 \\ \frac{v}{1-v} & \frac{1}{1-v} & 0 & 0 & 0 \\ 0 & 0 & \frac{\lambda}{2} & 0 & 0 \\ 0 & 0 & 0 & \frac{\lambda}{2} & 0 \\ 0 & 0 & 0 & 0 & \frac{1}{2} \end{bmatrix} \left(\begin{Bmatrix} \varepsilon_x \\ \varepsilon_y \\ \gamma_{yz} \\ \gamma_{xz} \\ \gamma_{xy} \end{Bmatrix} - \begin{Bmatrix} \alpha\Delta T \\ \alpha\Delta T \\ 0 \\ 0 \\ 0 \end{Bmatrix} \right). \tag{5}$$

The Young modulus is represented by E, the Poisson ratio by v, the letter α represents the coefficient of thermal expansion and the classical shear correction factor [14] $\lambda = 5/6$, is employed. Concerning the dependence of the mechanical properties on temperature, in Ref. [15] experimental tests were conducted on two steels. In one of the steels, it was observed that the modulus of elasticity does not change significantly from 25 to 250 °C; in the other steel, it was observed that from 20 to 200 °C the modulus of elasticity slightly decreases. Since only moderate temperature variations are considered in this work, it will be assumed that the material properties are constant. The parameter ΔT in Eq. (5) represents the temperature variation from the temperature of zero thermal stress.

The direct and membrane shear strain components are given by

$$\begin{Bmatrix} \varepsilon_x \\ \varepsilon_y \\ \gamma_{xy} \end{Bmatrix} = \begin{bmatrix} 1 & 0 & 0 & -z & 0 & 0 \\ 0 & 1 & 0 & 0 & -z & 0 \\ 0 & 0 & 1 & 0 & 0 & -z \end{bmatrix} \left(\begin{Bmatrix} \boldsymbol{\varepsilon}_0^{\mathbf{p}} \\ \boldsymbol{\varepsilon}_0^{\mathbf{b}} \end{Bmatrix} + \begin{Bmatrix} \boldsymbol{\varepsilon}_{\mathbf{L}}^{\mathbf{p}} \\ 0 \end{Bmatrix} \right), \tag{6}$$

where the linear membrane and bending strains, $\boldsymbol{\varepsilon}_0^{\mathbf{p}}$ and $\boldsymbol{\varepsilon}_0^{\mathbf{b}}$, and the geometrically nonlinear membrane strain, $\boldsymbol{\varepsilon}_{\mathbf{L}}^{\mathbf{p}}$, are

$$\boldsymbol{\varepsilon}_0^{\mathbf{p}} = \begin{Bmatrix} u^0_{,x} \\ v^0_{,y} \\ u^0_{,y} + v^0_{,x} \end{Bmatrix}, \quad \boldsymbol{\varepsilon}_0^{\mathbf{b}} = \begin{Bmatrix} -\dfrac{\partial \theta^0_y}{\partial x} \\ \dfrac{\partial \theta^0_x}{\partial y} \\ -\dfrac{\partial \theta^0_y}{\partial y} + \dfrac{\partial \theta^0_x}{\partial x} \end{Bmatrix}, \quad \boldsymbol{\varepsilon}_{\mathbf{L}}^{\mathbf{p}} = \begin{Bmatrix} \left(w^0_{,x}\right)^2 \Big/ 2 \\ \left(w^0_{,y}\right)^2 \Big/ 2 \\ w^0_{,x} w^0_{,y} \end{Bmatrix}. \tag{7}$$

The relations between the transverse shear strains and the displacements and rotations are the following:

$$\begin{Bmatrix} \gamma_{zx} \\ \gamma_{yz} \end{Bmatrix} = \begin{Bmatrix} w^0_{,x} + \theta_y \\ w^0_{,y} - \theta_x \end{Bmatrix}. \tag{8}$$

Adding the virtual work of the inertia, internal and external forces, and representing the dissipation by a matrix proportional to the linear stiffness matrix, the equations of motion are obtained:

$$\begin{bmatrix} \mathbf{M}_{\mathbf{p}}^{11} & 0 & 0 & 0 & 0 \\ 0 & \mathbf{M}_{\mathbf{p}}^{22} & 0 & 0 & 0 \\ 0 & 0 & \mathbf{M}_{\mathbf{p}}^{33} & 0 & 0 \\ 0 & 0 & 0 & \mathbf{M}_{\mathbf{Rx}}^{44} & 0 \\ 0 & 0 & 0 & 0 & \mathbf{M}_{\mathbf{Ry}}^{55} \end{bmatrix} \begin{Bmatrix} \ddot{\mathbf{q}}_u \\ \ddot{\mathbf{q}}_v \\ \ddot{\mathbf{q}}_w \\ \ddot{\mathbf{q}}_{\theta_x} \\ \ddot{\mathbf{q}}_{\theta_y} \end{Bmatrix} + \begin{bmatrix} \mathbf{K}_{1\mathbf{p}}^{11} & 0 & 0 & 0 & 0 \\ 0 & \mathbf{K}_{1\mathbf{p}}^{22} & 0 & 0 & 0 \\ 0 & 0 & \mathbf{K}_{1\gamma}^{33} - \mathbf{K}_{1\Delta\mathbf{T}}^{33} & \mathbf{K}_{1\gamma}^{34} & \mathbf{K}_{1\gamma}^{35} \\ 0 & 0 & \mathbf{K}_{1\gamma}^{43} & \mathbf{K}_{1\mathbf{b}}^{44} + \mathbf{K}_{1\gamma}^{44} & \mathbf{K}_{1\mathbf{b}}^{45} \\ 0 & 0 & \mathbf{K}_{1\gamma}^{53} & \mathbf{K}_{1\mathbf{b}}^{54} & \mathbf{K}_{1\mathbf{b}}^{55} + \mathbf{K}_{1\gamma}^{55} \end{bmatrix} \begin{Bmatrix} \mathbf{q}_u \\ \mathbf{q}_v \\ \mathbf{q}_w \\ \mathbf{q}_{\theta_x} \\ \mathbf{q}_{\theta y} \end{Bmatrix}$$

$$+\beta\begin{bmatrix} \mathbf{K}_{1\mathbf{p}}^{11} & 0 & 0 & 0 & 0 \\ 0 & \mathbf{K}_{1\mathbf{p}}^{22} & 0 & 0 & 0 \\ 0 & 0 & \mathbf{K}_{1\gamma}^{33}-\mathbf{K}_{1\Delta\mathbf{T}}^{33} & \mathbf{K}_{1\gamma}^{34} & \mathbf{K}_{1\gamma}^{35} \\ 0 & 0 & \mathbf{K}_{1\gamma}^{43} & \mathbf{K}_{1\mathbf{b}}^{44}+\mathbf{K}_{1\gamma}^{44} & \mathbf{K}_{1\mathbf{b}}^{45} \\ 0 & 0 & \mathbf{K}_{1\gamma}^{53} & \mathbf{K}_{1\mathbf{b}}^{54} & \mathbf{K}_{1\mathbf{b}}^{55}+\mathbf{K}_{1\gamma}^{55} \end{bmatrix}\begin{Bmatrix} \dot{\mathbf{q}}_{\mathbf{u}} \\ \dot{\mathbf{q}}_{\mathbf{v}} \\ \dot{\mathbf{q}}_{\mathbf{w}} \\ \dot{\mathbf{q}}_{\theta_{\mathbf{x}}} \\ \dot{\mathbf{q}}_{\theta_{\mathbf{y}}} \end{Bmatrix}+\begin{bmatrix} 0 & 0 & \mathbf{K}_2^{13}(\mathbf{q}_{\mathbf{w}}) & 0 & 0 \\ 0 & 0 & \mathbf{K}_2^{23}(\mathbf{q}_{\mathbf{w}}) & 0 & 0 \\ \mathbf{K}_3^{31}(\mathbf{q}_w) & \mathbf{K}_3^{32}(\mathbf{q}_{\mathbf{w}}) & \mathbf{K}_4^{33}(\mathbf{q}_{\mathbf{w}}) & 0 & 0 \\ 0 & 0 & 0 & 0 & 0 \\ 0 & 0 & 0 & 0 & 0 \end{bmatrix}\begin{Bmatrix} \mathbf{q}_{\mathbf{u}} \\ \mathbf{q}_{\mathbf{v}} \\ \mathbf{q}_{\mathbf{w}} \\ \mathbf{q}_{\theta_{\mathbf{x}}} \\ \mathbf{q}_{\theta_{\mathbf{y}}} \end{Bmatrix}$$

$$=\begin{Bmatrix} \mathbf{P}_u \\ \mathbf{P}_v \\ \mathbf{P}_w \\ \mathbf{M}_{\theta_x} \\ \mathbf{M}_{\theta_y} \end{Bmatrix}+\begin{Bmatrix} \mathbf{F}_{\mathbf{u}}^{\Delta T} \\ \mathbf{F}_{\mathbf{v}}^{\Delta T} \\ 0 \\ 0 \\ 0 \end{Bmatrix}. \tag{9}$$

In the former system of equations of motion, matrices of type $\mathbf{M}$ are mass matrices and matrices of type $\mathbf{K}_1$ are constant stiffness matrices. Matrices of type $\mathbf{K}_2(\mathbf{q_w})$, $\mathbf{K}_3(\mathbf{q_w})$ and $\mathbf{K}_4(\mathbf{q_w})$ depend on the transverse generalized coordinates, $\mathbf{q_w}$, and originate nonlinear terms. The letter β represents the factor of proportionality used to form the damping matrix and the vectors on the right-hand side represent forces of mechanical and thermal origin.

The matrices and vectors present in the former equation can be found in Ref. [10], with the exception of the matrices and vectors due to thermal effects, which, for uniform temperature variation from a reference temperature for zero thermal stresses, ΔT, are given by

$$\mathbf{F}_{\mathbf{u}}^{\Delta\mathbf{T}}=-\frac{Eh\alpha\Delta T}{1-\nu}\int_{\Omega}\mathbf{N}_{,x}^{u}\,\mathbf{d}\Omega, \tag{10}$$

$$\mathbf{F}_{v}^{\Delta\mathbf{T}}=-\frac{Eh\alpha\Delta T}{1-\nu}\int_{\Omega}\mathbf{N}_{,\mathbf{y}}^{\mathbf{v}}\,\mathbf{d}\Omega, \tag{11}$$

$$\mathbf{K}^{\Delta\mathbf{T}}=-\frac{Eh\alpha\Delta T}{1-\nu}\int_{\Omega}\mathbf{N}_{,\mathbf{x}}^{\mathbf{w}}\mathbf{N}_{,\mathbf{x}}^{\mathbf{w}^{\mathbf{T}}}+\mathbf{N}_{,\mathbf{y}}^{\mathbf{w}}\mathbf{N}_{,\mathbf{y}}^{\mathbf{w}^{\mathbf{T}}}\,\mathbf{d}\Omega. \tag{12}$$

In the former equations $\mathbf{N}^{\mathbf{u}}$, $\mathbf{N}^{\mathbf{v}}$ and $\mathbf{N}^{\mathbf{w}}$ are the vectors of shape functions associated with displacement components in the x, y and z directions, respectively.

The mechanical excitations applied here are uniformly distributed, transverse to the plate and with a sinusoidal variation in time. The nonlinear equations of motion are solved in the time domain by Newmark's method, with Newmark's parameters [14]. This is an implicit method, which, unlike explicit schemes allows one to update the nonlinear stiffness matrix until the equation

$$(\mathbf{Kl}+\mathbf{Knl}(\mathbf{q}_{wt_i+\Delta t})+a_0\mathbf{M}+a_1\mathbf{C})\mathbf{q}_{t_i+\Delta t}=\mathbf{P}_{t_i+\Delta t}+\mathbf{M}(a_0\mathbf{q}_{t_i}+a_2\dot{\mathbf{q}}_{t_i}+a_3\ddot{\mathbf{q}}_{t_i})+\mathbf{C}(a_1\mathbf{q}_{t_i}+a_4\dot{\mathbf{q}}_{t_i}+a_4\ddot{\mathbf{q}}_{t_i}) \tag{13}$$

is satisfied below a desired error condition. In the former equation $\mathbf{Kl}$ and $\mathbf{Knl}$ stand for the complete linear and nonlinear stiffness matrix, respectively; $\mathbf{M}$ and $\mathbf{C}$ represent the complete mass and damping matrices. The vectors P and q are the vectors of external forces and generalized coordinates. Although the constants a_0–a_5 are equal to the ones used in the application of Newmark's method to linear systems, and are textbook material, they are given here for the sake of completeness:

$$\delta=0.5,\quad \gamma=0.25,\quad a_0=\frac{1}{\gamma\Delta t^2},\quad a_1=\frac{\delta}{\gamma\Delta t},\quad a_2=\frac{1}{\gamma\Delta t},$$

$$a_3=\frac{1}{2\gamma}-1,\quad a_4=\frac{\delta}{\gamma}-1,\quad a_5=\left(\frac{\delta}{\gamma}-2\right)\frac{\Delta t}{2},\quad a_6=(1-\delta)\Delta t,\quad a_7=\delta\Delta t.$$

The repeated update of the nonlinear stiffness matrix until convergence is achieved is a process that is more time consuming in h-version than in p-version finite element models. This occurs because in the p-version both

the number of degrees of freedom and the number of elements are smaller than in the *h*-version, reducing the time spent in the assembly stage—actually, for simple geometries as is the case here, just one element is required. The fact that the *p*-version models generally have less degrees of freedom than *h*-version models, also means that less time is required to solve the system of equations that arises in each step of the implicit iterative procedure.

3. Applications

Steel plates with material properties $E = 21.0 \times 10^{10}\,\mathrm{N/m^2}$, $\nu = 0.3$, $\rho = 7800\,\mathrm{kg/m^3}$ and $\alpha = 18 \times 10^{-6}\,\mathrm{K^{-1}}$, are analysed. The letter ρ represents the mass density, the other symbols were already defined. In all numerical applications the width and length are $a = 0.5\,\mathrm{m}$ and $b = 0.5\,\mathrm{m}$, respectively. In the first set of examples the thickness is $h = a/240$. This plate will be referred to as Plate 1 and was chosen in order to compare results from this model with results from other references, as explained in the following paragraph. In the second and third sets of examples the plate thickness is changed to $a/h = 50$ (Plate 2) and $a/h = 30$ (Plate 3). The boundaries are fully clamped in all numerical tests (no rotation, transverse or in-plane displacement are possible at the boundaries); in this case, the first four linear natural frequencies of the $a/h = 240$ plate (Plate 1) are 470.77, 960.25, 960.25 and 1415.8 rad/s. The model used has a total of 123 degrees of freedom, after condensation of the equations of motion [10]; it provides a good approximation to the first natural frequencies and mode shapes.

Some tests were carried out to validate the model. First it was verified that the linear natural frequencies computed agree with the ones given in Ref. [16]. Next, the displacement amplitude of the forced response, in the absence of thermal effects, was compared with published values [17,18]. The agreement was close, except when harmonics of the excitation frequency appeared in the response. These harmonics were not considered in Refs. [17,18].

It is important to compute the critical buckling temperature, ΔT_{crit} of the plates [1], because this temperature may be a frontier between different types of dynamic responses. With this purpose two approaches were followed. The first was to solve an eigenvalue problem, where ΔT_{crit} is the eigenvalue, using the *p*-version FEM model. The second, simpler approach, was to employ Galerkin's method, follow thin plate theory and accept as a representation of the deformed shape of the plate a product of functions in x and y, each one equal to a clamped–clamped beam first mode shape [1]. The value obtained for the critical buckling temperature of Plate 1 was $\Delta T_{\mathrm{crit}} = 3.235\,\mathrm{K}$ with the *p*-version FEM (five out-of-plane and seven rotational shape function; details about these functions can be found in Refs. [10,12]), and $\Delta T_{\mathrm{crit}} = 3.276\,\mathrm{K}$ with the one degree of freedom, thin plate, Galerkin approach.

3.1. Plate 1, proportional damping factor equal to 10^{-4}

It is not intended here analyse in depth damping models and, as seen in Eq. (9), a simple proportional viscous damping model is followed. However, before stepping into the numerical applications, some words regarding damping are appropriate. In what concerns structural damping due to hysteresis, experiments referred by other authors (for example, Ref. [19]) indicate that the damping force is independent of frequency. In these cases the loss factor η is usually employed to quantify damping, and the amplitude of the damping force is, in a one degree of freedom system, given by $\eta K x(t)$, where K is the stiffness and $x(t)$ the displacement. According to Ref. [19] the values of the loss factor for steel may vary from 0.001 to 0.008.

Damping in a structure is also largely influenced by boundary conditions, including interaction with air, leading to a great case dependency of the amount and type of damping that should be considered. In Ref. [20] a viscous damping model was used and the value 0.5% is referred as an appropriate value for the damping factor; however, values close to 1.9%, that is four times more, were measured (this values refer to aluminium, but it is expected that a large influence of the mounting procedures and other factors also occurs is steel specimens). The relation between the damping factor employed in the present work, β and the viscous damping ratio, ζ, can be derived using a one degree of freedom model:

$$\beta = \frac{2\zeta}{\omega_n}. \tag{14}$$

The former comments justify that small damping factors β are employed here and that variations of its value are considered to analyse the influence that the amount of damping has on the nonlinear oscillations. In an application, measurements in a representative test structure or prototype are recommended to determine the best value to assume for β.

In the first set of examples, the value $\beta = 10^{-4}$ is used for the damping parameter. The aim of these examples is to see how Plate 1, which is a thin plate, behaves for different temperatures.

Fig. 1 shows the large influence that relatively small temperature changes can have in the dynamic behaviour of Plate 1. The excitation amplitude is 250 N/m^2 and the excitation frequency is 472 rad/s. This value of the excitation frequency is slightly higher than the linear natural frequency (470.77 rad/s), and was chosen because the unheated plate experiments a hardening spring effect due to large amplitude vibrations. Nevertheless, it is acknowledged that the difference between the frequencies is minor, and it was later verified that excitations at 470.77 or 472 rad/s give approximately the same response.

At 3.5 and 4 K, i.e., very near the critical temperature, the phase plots are approximately elliptical and the Poincaré section consists of a sole point (these plots are not shown), which proves that the motion is still very close to harmonic. However, as the temperature increases and in spite of the small excitation amplitude, motions which are far from harmonic occur. Fig. 2 shows the phase plots and the Poincaré sections of oscillations for temperature variations equal to 10 and 20 K. Data were computed for many cycles of the excitation, to allow the transients to dissipate.

For a clamped plate, the nonlinear strain–displacement relations of von Kármán are usually considered to be valid until a ratio of maximum deflection to thickness equal to 2 (Ref. [21], where thin plate theory is employed). Therefore, the displacements at 20 K shown in Fig. 2, give an indication about the behaviour of the plate at larger temperatures, but may be too large for the present model to be precise. On the other hand, also in Ref. [21], the von Kármán strain–displacement relations provided results comparable to experiments up to a deflection-to-thickness ratio equal to 6.

It should be pointed out that Fig. 2(c) is somewhat misleading, since it appears to be a neat closed line. However, a zoom showed that it is not. The Poincaré sections represented in Fig. 2 are either formed by a finite, but large, number of points in which case the motion is periodic with harmonics of the excitation frequency or they tend to a closed line, which would indicate that the oscillations are quasi-periodic. The latter would justify why it was not possible to detect a closure of the line in the phase plot. The frequency spectrum of this signal will remove the doubt concerning the type of oscillation.

In the frequency spectra represented in Fig. 3 the vertical axis gives the amplitude of the displacement in the z direction divided by the thickness of the plate. When the temperature rise is 4 K, the frequency spectrum

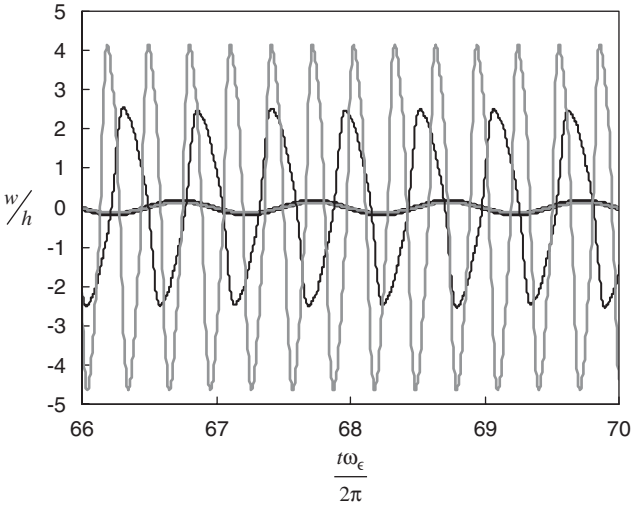

Fig. 1. Displacement time history of Plate 1 mid-point; excitation at 472 rad/s, 250 N/m^2. Temperature change, ΔT : ▬ 3.5 K, ▬ 4 K, — 10 K, ▬ 20 K.

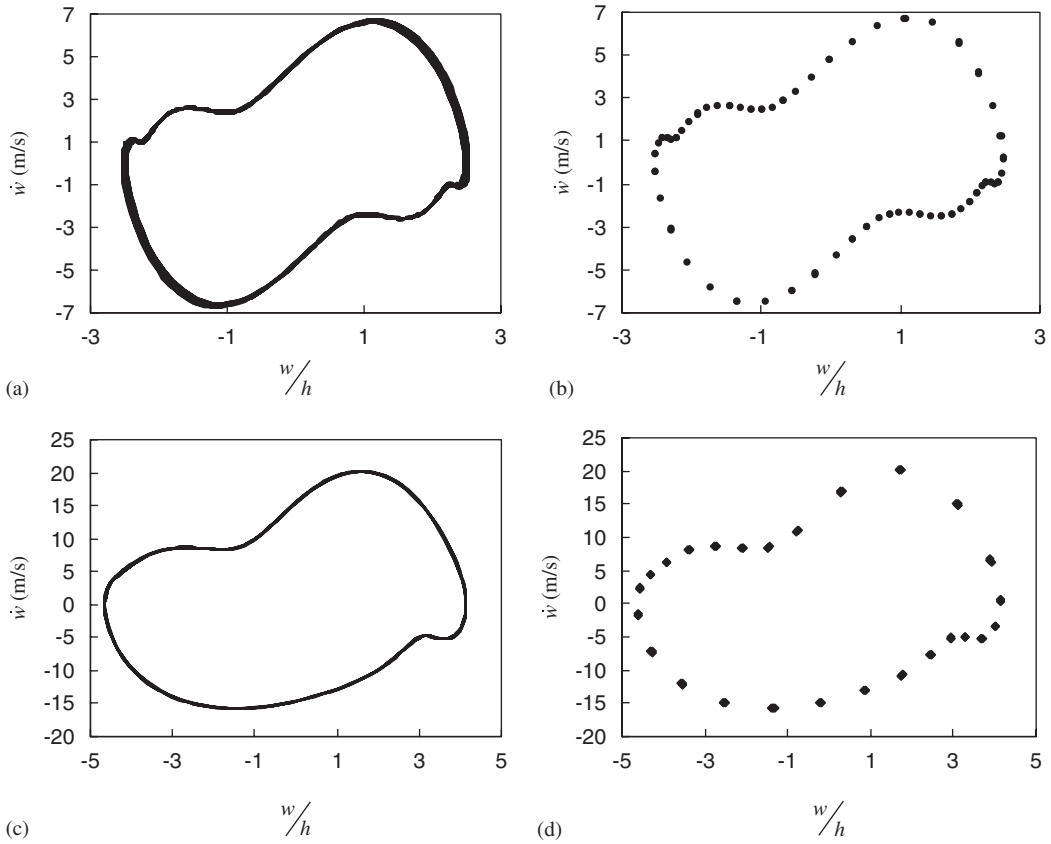

Fig. 2. Plate 1 mid-point, excitation 250 N/m^2, 472 rad/s: $\Delta T = 10$ K (a) Phase plot and (b) Poincaré section a $\Delta T = 20$ K (c) Phase plot and (d) Poincaré section.

presents a sole spike, at the excitation frequency. The other plots have several spikes which are approximately related by integer values; hence, the spectra are typical of periodic oscillations. In the case of the 10 K temperature variations, the major peaks occur at the first harmonic and at odd harmonics of the first, there is no constant term. However, in the 20 K case, both odd and even harmonics appear as well as the constant term. This confirms that at 20 K the plate is not oscillating about $w = 0$, i.e., the plate is not oscillating about a flat equilibrium position and that the property of reflection or inversion symmetry (Ref. [22], p. 466) was lost. Therefore, there is a difference in the largest positive and negative amplitudes when $\Delta T = 20$ K, which was also evident in Fig. 2. It is recalled that when buckling occurs, the flat equilibrium configuration becomes unstable and new stable equilibrium configurations appear.

There is a relation between the type of motion (harmonic or not harmonic) and the shapes assumed by the plate. In fact, for $\Delta T = 3.5$ and 4 K, the most prominent mode is by far the first one, and when ΔT is equal to 10 and 20 K, higher order modes become very important.

3.2. Plate 1, proportional damping factor equal to 10^{-6}

In order to analyse the effect of damping, the vibrations of Plate 1 with a smaller damping parameter are analysed. The frequency and amplitude of the distributed force are equal to the ones of the previous section (472 rad/s and 250 N/m^2). Different temperature changes ΔT are assumed, the first is a temperature rise equal to 4 K.

The time plot of the middle point oscillations, when the damping parameter is 10^{-4}, was given in the previous section. In this case, the plate oscillates symmetrically with respect to its flat configuration, and the oscillations are sinusoidal in time (naturally, the Fast Fourier Transform, originated a single spike at the

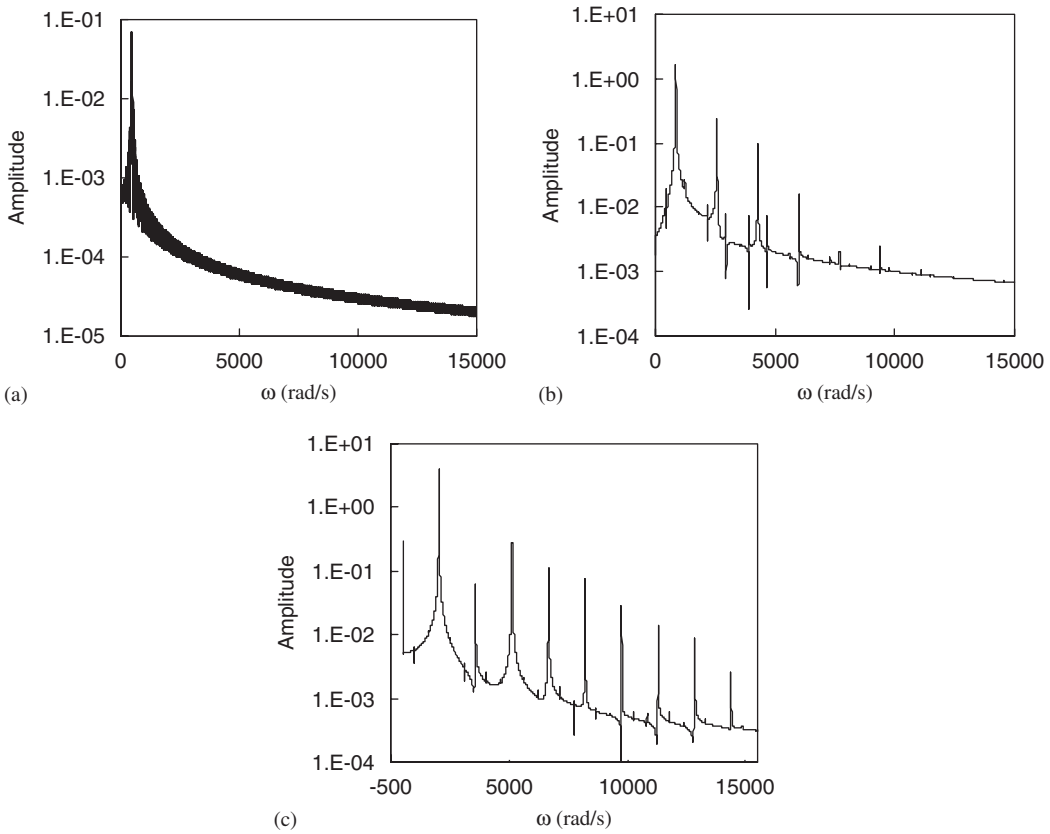

Fig. 3. Fourier spectra of Plate 1 mid-point displacement, excitation $250\,\mathrm{N/m^2}$, at 472 rad/s: (a) $\Delta T = 4\,\mathrm{K}$, (b) $\Delta T = 10\,\mathrm{K}$ and (c) $\Delta T = 20\,\mathrm{K}$.

excitation frequency and the phase plot, which was not shown, is an ellipse). However, if the damping parameter is decreased to $\beta = 10^{-6}$, the oscillations turn out to be quite irregular, as shown in Fig. 4. Just the first 20 cycles of the time history are shown, because they allow one to see the evolution of the response and because very large amplitude displacements were already achieved, and the model may cease to be valid. Although it is not shown in this figure, data was obtained until the 300th cycle of the excitation and the motion found was always extremely irregular. This irregularity can also be verified in the phase plot and in the representation of the Poincaré map (Fig. 4). The spectrum of this signal was computed using 2^{14} points, collected at $3.32 \times 10^{-5}\,\mathrm{s}$. There are no closed lines in the phase and Poincaré plots and the amplitude spectrum has a broadband character; these are characteristics of chaotic oscillations [22]. Although the excitation frequency is very close to the first linear natural frequency, it is verified that higher order modes are very important in the motions (Fig. 5).

The time step employed in the Newmark integration scheme to obtain the data shown in Figs. 4 and 5, was $\Delta t = 10^{-7}\,\mathrm{s}$, that is more than 133,000 points per period of the excitation force (which is $1.331183\,10^{-2}\,\mathrm{s}$). In spite of this very refined discretization in time, integrations with smaller time steps were carried out, in order to verify the reliability of the results. Along the complete time spans of the integrations, the data obtained with the different time steps has very similar characteristics, in what amplitudes and irregularity of the motion are concerned. For the first cycles, the data obtained with smaller time steps is indeed equal to the one obtained with $\Delta t = 10^{-7}\,\mathrm{s}$. However, in another signature of chaotic motions, sooner or later the data computed with different time steps deviate from each other. Fig. 6 demonstrates what was just said (note that one of the curves was computed using 2,662,367 points per excitation cycle).

Computation of the largest Lyapunov exponent was carried out, using the algorithm given in Ref. [23] for time series. Positive values, an indication of chaos, were computed but the actual values obtained are not given

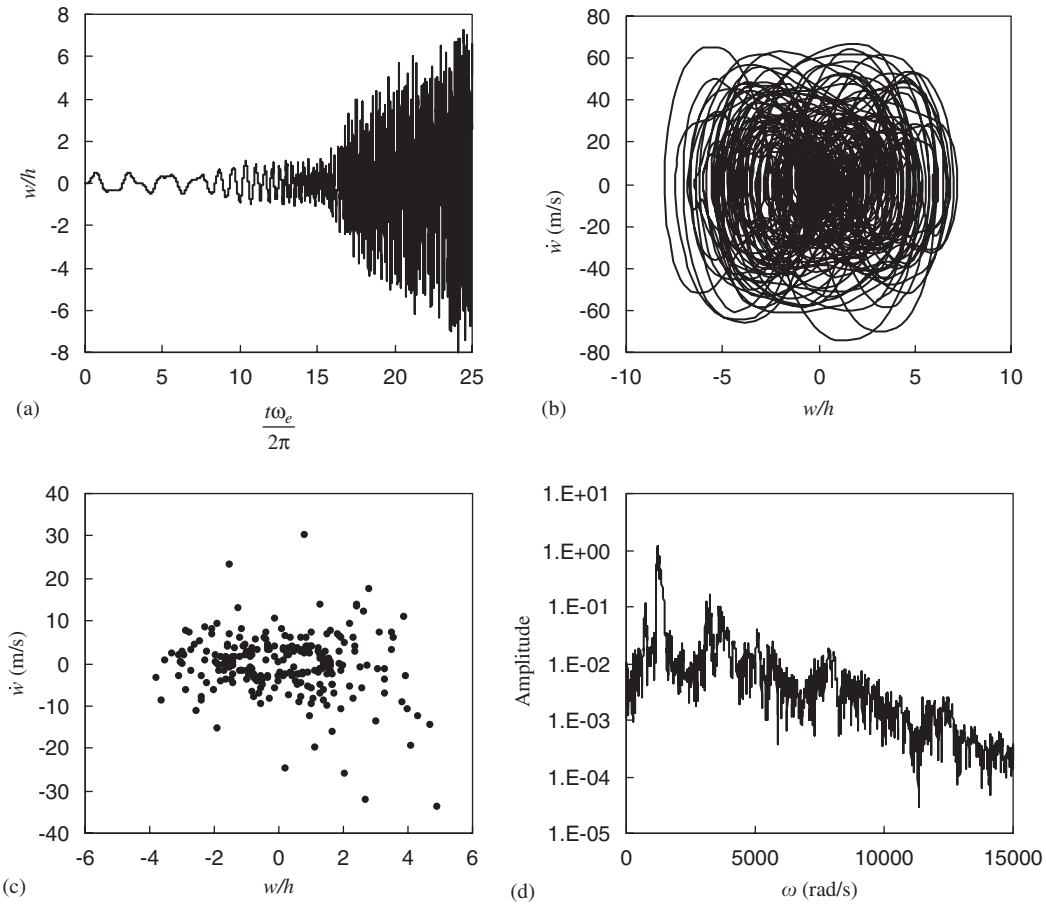

Fig. 4. Time history (a), phase plot (b), Poincaré section (c) and amplitude spectrum (d) of Plate 1 mid-point oscillation (472 rad/s, 250 N/m^2, 4 K, $\beta = 10^{-6}$).

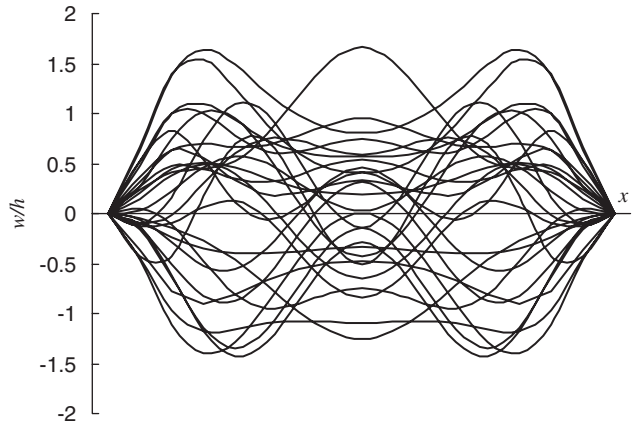

Fig. 5. Sections $y = 0$ of Plate 1 at different instants (472 rad/s, 250 N/m^2, 4 K, $\beta = 10^{-6}$).

here, because they depended on the algorithm parameters—parameters like embedding dimension, time delay and others defined in Ref. [23]. This dependence seems to be a normal occurrence with the algorithm employed, but it probably was increased by the numerical errors (shown in Fig. 6), which are added to the

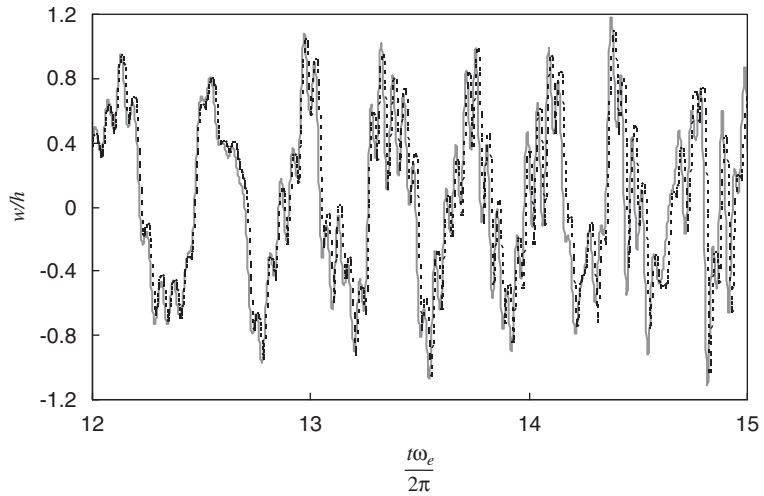

Fig. 6. Time plots of Plate 1 mid-point displacement (472 rad/s, 250 N/m^2, 4 K, $\beta = 10^{-6}$): — $\Delta t = 1 \times 10^{-7}$ s (133,118 points per excitation cycle); ---- $\Delta t = 5 \times 10^{-9}$ s (2,662,367 points per excitation cycle).

instabilities of the chaotic oscillation in the definition of the time signal. The same algorithm was used in periodic and quasi-periodic oscillations that occurred in this study, and it was found that the largest Lyapunov exponent is zero, as should be in these cases.

The latter highly irregular motion was not found with a damping parameter equal to 10^{-4}. Therefore, with the lower damping parameter the fact that the critical temperature was passed becomes much more important.

In order to verify the influence of damping on the response, another example in Plate 1 was explored; this time the temperature variation was below the critical one, namely $\Delta T = 2$ K, but with very low damping (again $\beta = 10^{-6}$). Computations were carried out until the 225 cycles of excitation and the motion found presented a beating like phenomenon, which was dissipating very slowly, due to the small damping. In terms of deformation, the first mode shape was strongly dominant. In conclusion, also with a very small damping, the motion has a far more regular nature below the critical temperature ($\Delta T = 2$ K) than above the critical temperature ($\Delta T = 4$ K).

3.3. Plate 2

All geometric parameters of Plate 2 are similar to the ones of Plate 1, except the thickness which is $h = 0.01$ m ($a/h = 50$). The critical buckling temperature in this case rises to $\Delta t_{\text{crit}} \approx 74$ K (74.06 K with the p-version FEM model and 75.48 K with the one degree of freedom Galerkin's method). The first linear natural frequencies are 2250.2, 4575.3, 4575.3, 6726.6 and 8173.5 rad/s. In this subsection the damping factor is $\beta = 10^{-6}$ except when written otherwise.

In Plate 1, when $\Delta T = 10$ K, the oscillations were quite irregular, particularly so if $\beta = 10^{-6}$. However, Plate 2 is 4.8 times thicker, and much less influenced by temperature rises. The following figure gives the response to a force of 250 $(h_2/h_1)^3$ N/m^2 (that is 27,648 N/m^2); this relation between the amplitudes of the excitation applied to the two plates was chosen because the bending stiffness is proportional to h^3. Some numerical tests were carried out slightly varying the excitation frequency around the fundamental frequency of the unheated plate. No significant variation in the response was obtained due to these small variations in the frequency of excitation, and henceforth the excitation frequency is always the first natural frequency of the unheated plate.

Fig. 7 represents the transverse displacement and the phase plots of the plate central point in two time windows. These show that convergence to a steady-state solution with low damping requires a large number of time steps, and care must be taken not to mistake a response still influenced by transients with a non-periodic response. This particular motion is in fact harmonic and at lower adimensional amplitude than its counterpart

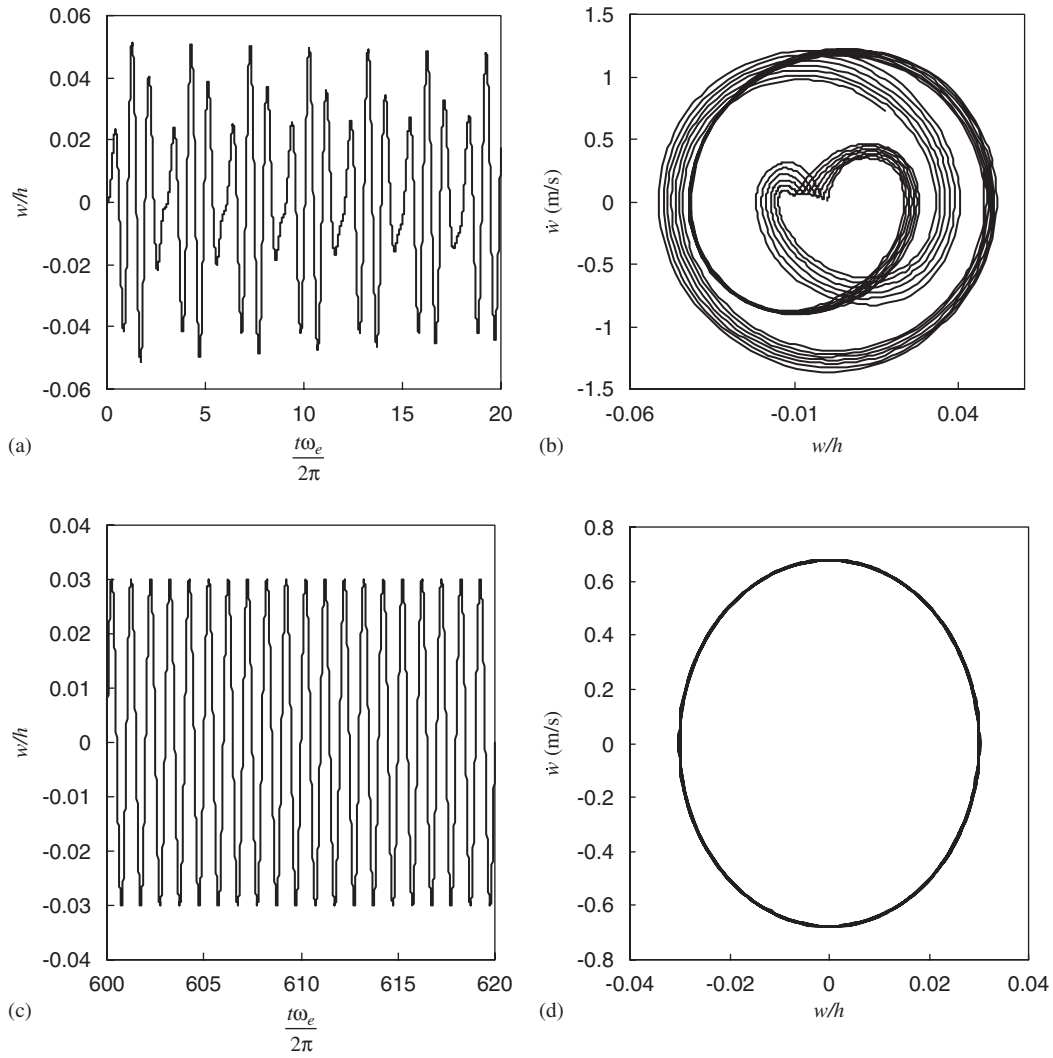

Fig. 7. Time (a and c) and phase (b and d) plots of Plate 2 mid-point oscillation ($\omega_{\ell 1}$, 250 $(h_2/h_1)^3$ N/m^2, 10 K, $\beta = 10^{-6}$).

oscillation of Plate 1. Fig. 8 is a representation of the Poincaré map, which differs from the usual 2D figure in the displacement and velocity, because a third axis was introduced to allow one to verify the evolution of the map with the number of excitation cycles. It is evident that the map tends to a point, a characteristic of 1-periodic motions.

The following figures are also related with the response to a force of 250 $(h_2/h_1)^3$ N/m^2, frequency $\omega_{\ell 1}$, but now the temperature rise is 80 K, that is above the critical buckling temperature of Plate 2. Fig. 9 represents the transverse displacement and the phase plots of the central point, well after transients dissipated. In the phase plot the response to one hundred excitation cycles is represented. In comparison with the former case, where the temperature was 10 K, it is immediately visible that the displacement amplitude is larger and that the oscillation is asymmetric with respect to the flat configuration of the plate.

Performing a fast Fourier transform on the data, just two relevant peaks are obtained (Fig. 9(c)), the first near 2251 rad/s and the second around 7885 rad/s. In fact, the first peak occurs at the excitation frequency $\omega = 2250.233$ rad/s, the small difference between this value and 2251 rad/s is due to errors in the FFT. The second peak occurs at approximately 3.503ω. This value is close to 7/2, but in spite of the small uncertainties, due to discretization, about the frequency values given by the FFT algorithm, we know that the relation

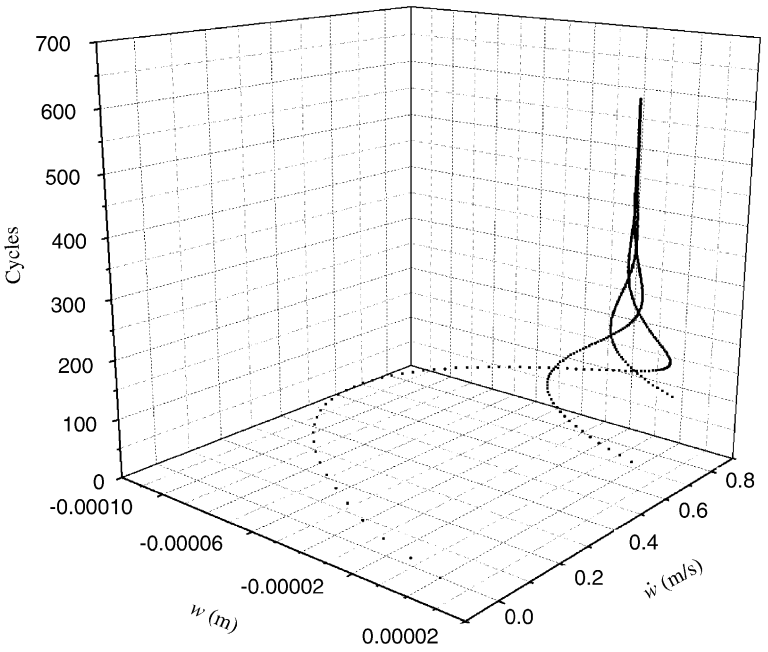

Fig. 8. Tridimensional representation of Poincaré map of Plate 2 mid-point oscillation ($\omega_{\ell 1}$, 250 $(h_2/h_1)^3$ N/m^2, 10 K, $\beta = 10^{-6}$).

between the frequencies is not 7/2. In fact, the frequencies should be incommensurate, otherwise the phase plot would be a closed line, as the one represented in Fig. 10. Thus, the oscillation is a two period quasiperiodic one, which also agrees with the fact that the Poincaré section presents an uncountable multitude of points[1] (also represented in Fig. 9). An inspection of the shapes assumed by the plate along time showed that the first and one higher order mode are present in the oscillation.

In a somewhat academic test, the excitation amplitude is increased to the very large value of 200,000 N/m^2, and the values of the damping factor, excitation frequency and temperature variation are kept at, respectively, $\beta = 10^{-6}$, $\omega_{\ell 1}$ and 80 K. In these conditions, the data represented in Fig. 11 was obtained, where the transverse displacement and velocity are again the ones of the middle point. One can see that this is a very irregular motion, more irregular than the one obtained in the same conditions but with lower excitation amplitude. The phase plot line does not seem to close and the number of points in the representation of the Poincaré map increases with the number of excitation cycles, indicating that this is probably not a periodic motion.[1] On the other hand, the highest Lyapunov exponent was computed using the program provided in Ref. [23] for time series. The value zero was found, which indicates that the motion is not chaotic.

In the Fourier spectrum there are peaks at certain frequencies, and sidebands around this peaks. The larger amplitude occurs around 3585 rad/s, which is larger than the excitation frequency and than the first natural frequency; moreover, it does not coincide with any linear natural frequency. The sidebands, which appear uniformly spaced around 314 rad/s apart, are a characteristic of quasi-periodic motions, according to Ref. [22]. The second peak is at 11,607 rad/s and sidebands, also at more or less 314 rad/s, appear again. Other peaks, of small amplitude, appear accompanied by sidebands. As occurred with the other motions found before and that were not harmonic, the first and at least one higher order mode are present in the response.

From the plots discussed in the two previous paragraphs and from the fact that the largest Lyapunov exponent is zero, one concludes that the oscillation is quasi-periodic.

A curious response is obtained if the above conditions are kept, but damping is almost zero (Fig. 12). In this case, the oscillations have all the characteristics of chaotic motions, as one can see in the following figures.

[1]The fact that the Poincaré section does not correspond to any simple geometrical form, does not, on its own, prove that the motion is not periodic [22].

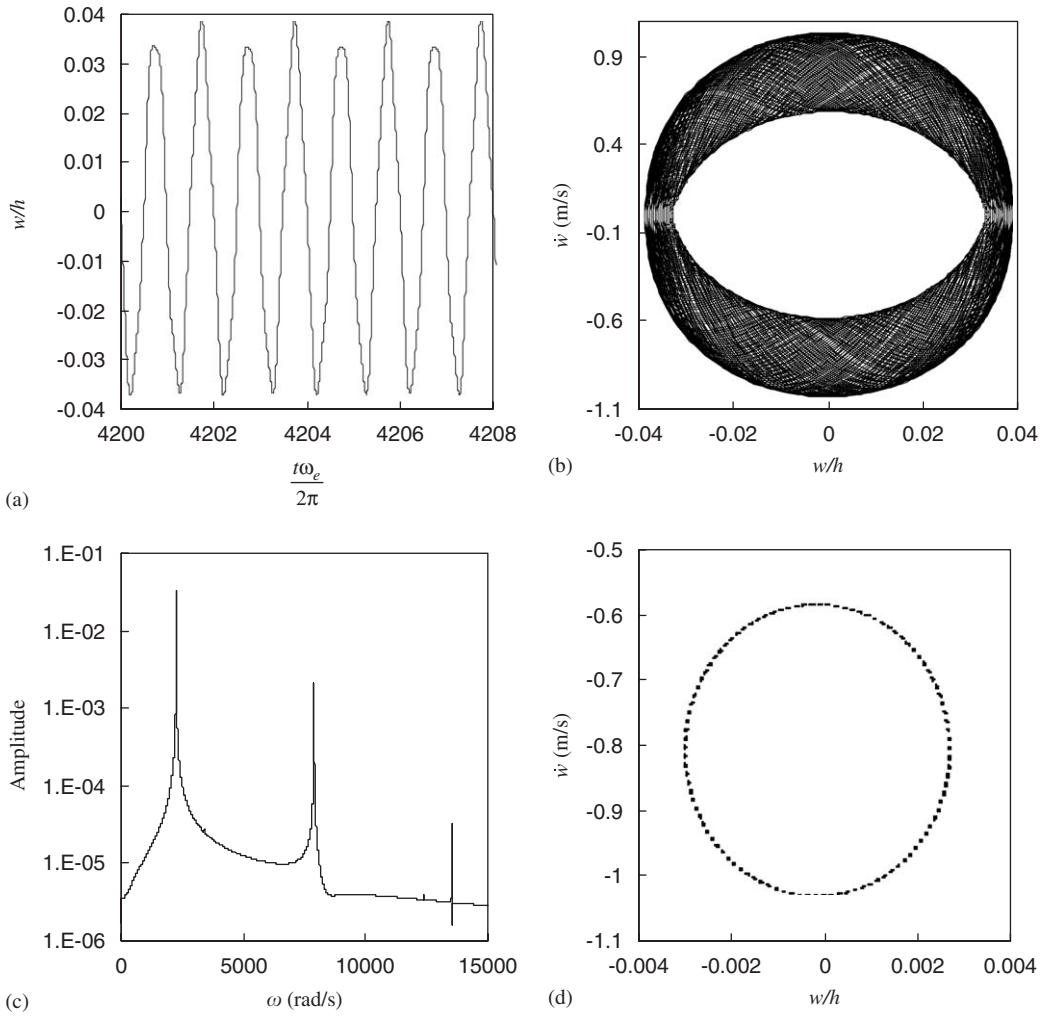

Fig. 9. (a) Time history, (b) phase plot, (c) amplitude spectrum and (d) Poincaré section of Plate 2 mid-point oscillation ($\omega_{\ell 1}$, 250 $(h_2/h_1)^3\,\mathrm{N/m^2}$, 80 K, $\beta = 10^{-6}$).

Moreover, independently of the, very small, time steps that were employed in the Newmark integration procedure, the amplitude of oscillation grows to very large values as time progresses. The particular results shown were computed with $\Delta t = 5 \times 10^{-9}$ s (around 558,450 points per excitation cycle) and in the time and phase plots just the first twenty cycles are shown. The oscillations contained the first and higher order modes. The large amplitudes of vibration displacement are shown in order to illustrate how the motion tends to evolve; nevertheless, the previous concerns about the validity of the model at the larger displacements are also applicable here.

3.4. Plate 3

Finally, to verify how the oscillations vary with the plate thickness, a plate with properties similar to the previous ones but where the thickness is $h = 0.0166667$ m, i.e., where $a/h = 30$, is briefly analysed. The critical buckling temperature in this case rises to $\Delta t_{\mathrm{crit}} \approx 203.30$ K (203.30 K with the p-version FEM model and 208.84 K with the one degree of freedom Galerkin's method and thin plate theory). In this subsection the damping factor is $\beta = 10^{-6}$.

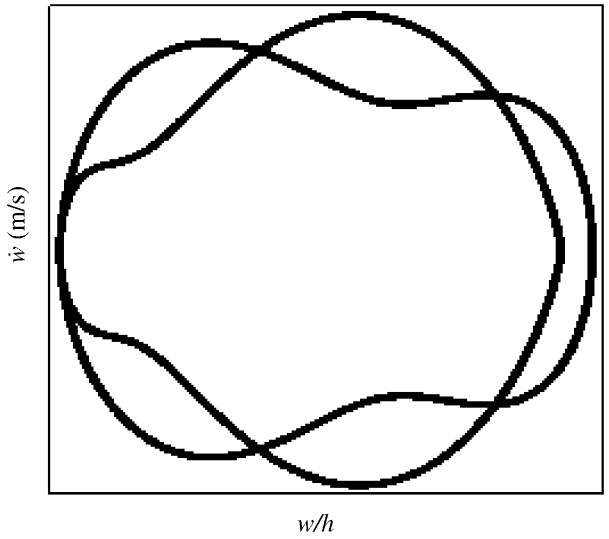

Fig. 10. Phase plot generated using an artificial time history with two frequencies, ω and 3.5ω.

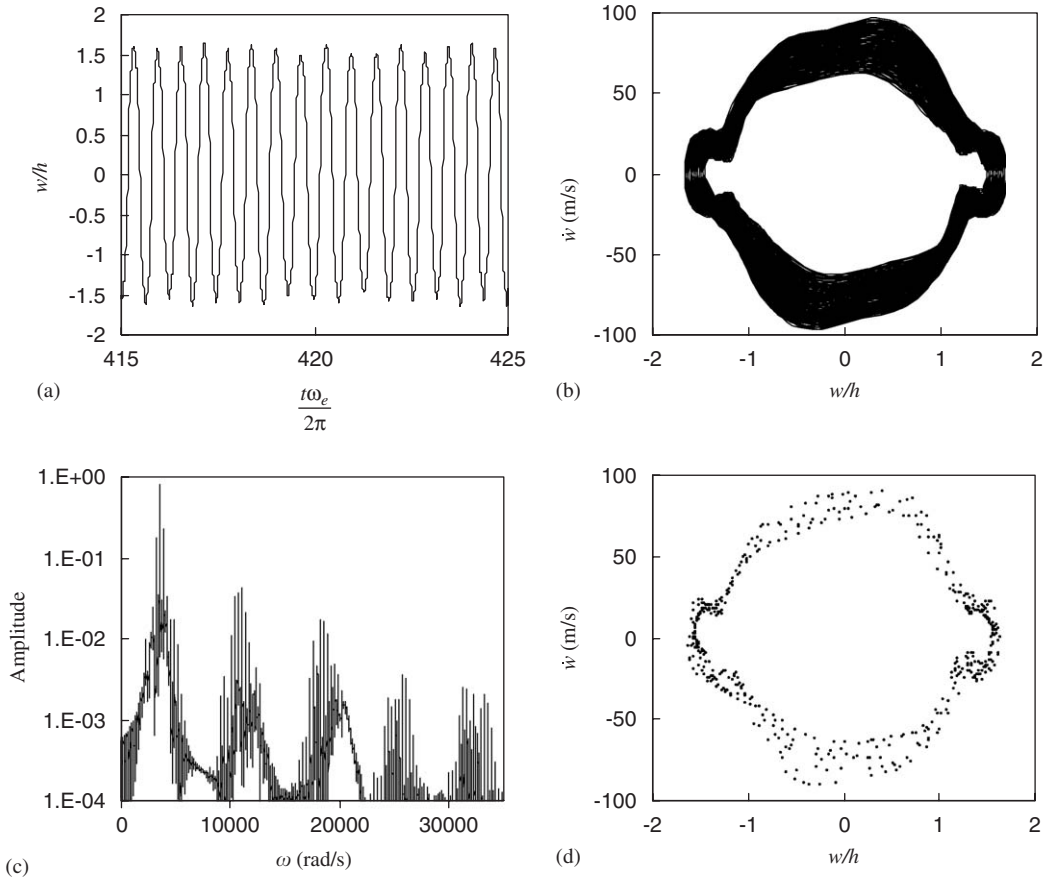

Fig. 11. (a) Time history, (b) phase plot, (c) amplitude spectrum and (d) Poincaré section of Plate 2 mid-point oscillation ($\omega_{\ell 1}$, 200,000 N/m^2, 80 K, $\beta = 10^{-6}$).

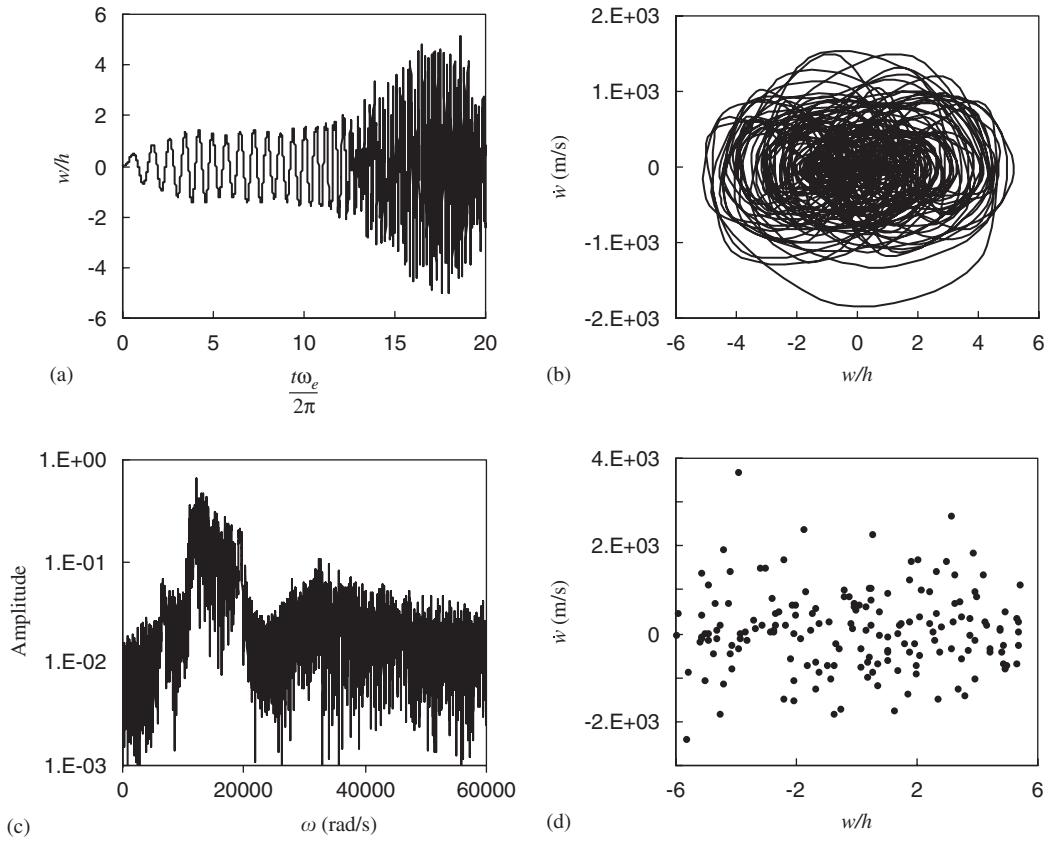

Fig. 12. (a) Time, (b) phase plot, (c) amplitude spectrum and (d) Poincaré section of Plate 2 mid-point oscillation ($\omega_{\ell 1}$, 200,000 N/m^2, 80 K, $\beta \approx 0$).

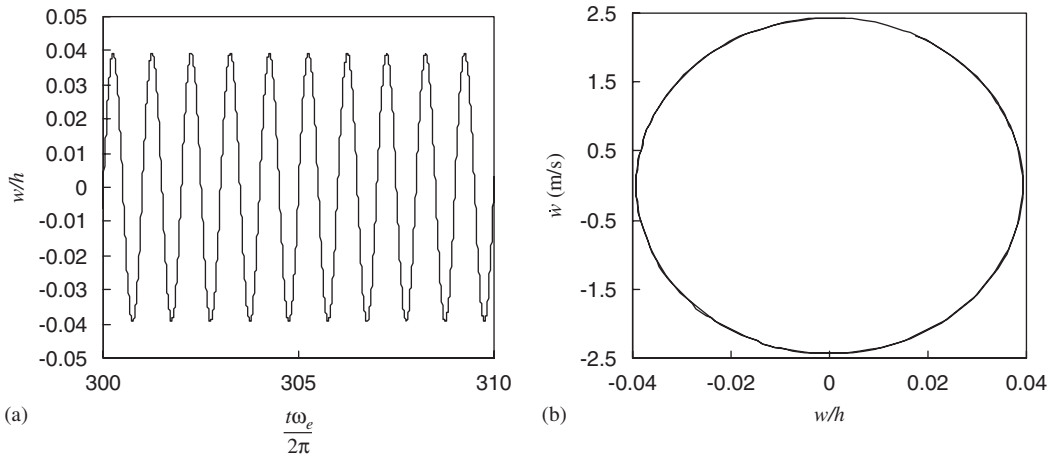

Fig. 13. (a) Time and (b) phase plot of Plate 3 mid-point oscillation ($\omega_{\ell 1}$, $(h_2/h_1)^3$ 250 N/m^2, 80 K, $\beta = 10^{-6}$).

The geometry, boundaries and excitations considered in this text are always symmetric with respect to the *xz* and *yz* planes. However, so far, symmetric and antisymmetric shape functions have been used to verify if antisymmetric modes are excited due to modal interactions. In all the numerical tests carried out, it was observed that the only transverse modes excited are the symmetric ones. Thus, in the following examples only

symmetric functions are used and the number of one-dimensional out-of-plane shape functions was reduced to four (16 bi-dimensional functions). It is stressed that, although only symmetric responses are studied, the existence of non-symmetric responses is not precluded.

The oscillations represented in Fig. 13 are due to a force with 250 $(h_3/h_1)^3$ N/m^2 (that is 1.28×10^5N/m^2) and frequency $\omega_{\ell 1}$. The damping parameter is $\beta = 10^{-6}$ and the temperature rise is 80 K, which is below the plate critical buckling temperature. The oscillations can be compared with the ones of Plates 1 and 2, which are, respectively, represented in Figs. 4 and 9; the conditions are similar, with the exception of the ΔT in Fig. 4, which is smaller, because very large displacements were attained. We see that, as the plate thickness increases, the motion passes from chaotic to quasiperiodic, and finally to periodic. This in spite of the fact that the force amplitude was increased by a factor of $(h_i/h_1)^3$, where i is 2 or 3.

Several, quite large, excitation amplitudes were applied to Plate 3, with a temperature above the plate critical buckling temperature, but chaotic oscillations were not found. Hence, it is apparent that it will be quite difficult in practice to achieve chaos in a thick plate.

4. Conclusion

A p-version plate finite element that accounts for shear deformation and rotary inertia was applied to study oscillations of plates under transverse harmonic excitations and thermal fields. In the numerical experiments, the excitation frequencies of the mechanical force were close or equal to the first linear natural frequency.

Larger temperatures facilitated the appearance of large amplitude vibrations. More significant than that, for different excitation amplitudes, for different excitation frequencies and for different damping factors it was verified that a temperature rise causes transitions from harmonic to non-harmonic, even to non-periodic, oscillations. These transitions are due to the in-plane forces that are introduced by temperature and that cause buckling, when the critical temperature is passed. After buckling, the flat equilibrium position becomes unstable and new stable equilibriums appear.

Non-periodic motions are much more likely if damping is small. For very small damping and for a temperature above the critical buckling temperature, oscillations were found that present several signals of chaotic vibrations, namely: the time plot does not repeat, the phase plot is not a closed line, the Poincaré section is constituted by a cloud of points and the frequency spectrum presents a broad-band character. Moreover, positive Lyapunov exponents were in this case computed, although the precise value of the exponents depended somewhat on the parameters used to compute them. Above the critical temperature, but with larger damping, the oscillations were periodic. As a result of chaotic systems characteristics, it is computationally demanding to obtain accurate values in a large time span using numerical integration, particularly when the system has many degrees of freedom.

It was demonstrated that, in the case of the multi-harmonic and of the non-periodic motions, higher order modes are very important, which justifies the use of shear deformation models for relatively thin plates. Moreover, the appearance of higher order modes in chaotic oscillations indicates that models with more degrees of freedom will be required for accuracy. Absence of symmetry of non-periodic and of some periodic oscillations with respect to the flat plate configuration (i.e., the xy plane) was also found. This is justified by the buckling of the plate that occurs when the temperature rises.

In the case of thick plates, non-periodic responses to harmonic transverse external forces are difficult to achieve. The explanation for this is that a thick plate requires a very large force, if its oscillations are to approach the various equilibrium positions (unstable and stable) that emerge after buckling.

References

[1] E.A. Thorton, *Thermal Structures for Aerospace Applications*, AIAA Education Series, Reston, 1996.

[2] J.H. Argyris, L. Tenek, Nonlinear and chaotic oscillations of composite plates and shells under periodic heat load, *Computer Methods in Applied Mechanics and Engineering* 122 (1995) 351–377.

[3] K.D. Murphy, L.N. Virgin, S.A. Rizzi, Characterizing the dynamic response of a thermally loaded, acoustically excited plate, *Journal of Sound and Vibration* 196 (1996) 635–658.

[4] Y.C. Shi, R.Y.Y. Lee, C. Mei, Thermal postbuckling of composite plates using the finite element modal coordinate method, *Journal of Thermal Stresses* 22 (1999) 595–614.
[5] J.M. Dhainaut, X.Y. Guo, C. Mei, S.M. Spottswood, H.F. Wolfe, Nonlinear random response of panels in an elevated thermal-acoustic environment, *Journal of Aircraft* 40 (2003) 683–691.
[6] G.F. Cheng, C. Mei, Finite element modal formulation for hypersonic panel flutter analysis with thermal effects, *AIAA Journal* 42 (2004) 687–695.
[7] K.D. Murphy, D. Ferreira, Thermal buckling of rectangular plates, *International Journal of Solids and Structures* 38 (2001) 3979–3994.
[8] R. Gilat, J. Aboudi, The Lyapunov exponents as a quantitative criterion for the dynamic buckling of composite plates, *International Journal of Solids and Structures* 39 (2002) 467–481.
[9] H. Chen, L.N. Virgin, Dynamic analysis of modal shifting and mode jumping in thermally buckled plates, *Journal of Sound and Vibration* 278 (2004) 233–256.
[10] P. Ribeiro, A hierarchical finite element for geometrically non-linear vibration of thick plates, *Meccanica* 38 (2003) 115–130.
[11] R.D. Mindlin, Influence of rotatory inertia and shear on flexural motions of isotropic, elastic plates, *Journal of Applied Mechanics* 18 (1951) 31–38.
[12] P. Ribeiro, M. Petyt, Nonlinear vibration of beams with internal resonance by the hierarchical finite element method, *Journal of Sound and Vibration* 224 (1999) 591–624.
[13] K.L. Verma, Thermoelastic vibrations of a transversely isotropic plate with thermal relaxations, *International Journal of Solids and Structures* 38 (2001) 8529–8546.
[14] M. Petyt, *Introduction to Finite Element Vibration Analysis*, Cambridge University Press, Cambridge, 1990.
[15] G.-Q. Li, S.-C. Jiang, Y.-Z. Yin, K. Chen, M.-F. Li, Experimental studies on the properties of constructional steel at elevated temperatures, *Journal of Structural Engineering, ASCE* 129 (2003) 1717–1721.
[16] A. Leissa, *Vibration of Plates*, Acoustical Society of America, 1993.
[17] P. Ribeiro, M. Petyt, Nonlinear vibration of plates by the hierarchical finite element and continuation methods, *International Journal of Mechanical Sciences* 41 (1999) 437–459.
[18] C. Mei, K. Decha-Umphai, A finite element method for non-linear forced vibrations of rectangular plates, *AIAA Journal* 23 (1985) 1104–1110.
[19] C.F. Beards, *Structural Vibration Analysis: Modelling, Analysis and Damping of Vibrating Structures*, Ellis Horwood Limited, Chichester, 1983.
[20] H. Wolfe, An experimental investigation of nonlinear behaviour of beams and plates excited to high levels of dynamic response, Ph.D. Thesis, University of Southampton, 1995.
[21] C.Y. Chia, *Nonlinear Analysis of Plates*, McGraw-Hill, New York, 1980.
[22] A.H. Nayfeh, B. Balachandram, *Applied Nonlinear Dynamics: Analytical, Computational, and Experimental Methods*, Wiley, New York, 1995.
[23] A. Wolf, J.B. Swift, H.L. Swinney, J.A. Vastano, Determining Lyapunov exponents from a time series, *Physica D* 16 (1985) 285–317.